RF signal detection and energy harvesting with a spin-torque diode having perpendicular magnetic anisotropy of the free layer

P. Yu. Artemchuk,[1] O. V. Prokopenko,[1, a)] E. Bankowski,[2] T. Meitzler,[2] V. S. Tyberkevych,[3] and A. N. Slavin[3]
[1)] *Faculty of Radio Physics, Electronics and Computer Systems, Taras Shevchenko National University of Kyiv, Kyiv 01601, Ukraine*
[2)] *Ground Vehicle Systems Center, Warren, Michigan 48397, USA*
[3)] *Department of Physics, Oakland University, Rochester, Michigan 48309, USA*

We demonstrate theoretically that the out-of-plane regime of operation of a spin-torque diode (SD) can be achieved for the frequencies $\lesssim 250$ MHz without any external bias DC magnetic field, if the SD's free layer has a perpendicular magnetic anisotropy of the first and second order. We also show that such a device can operate as a broadband energy harvester capable of converting of an incident RF power to a DC power with conversion efficiency $\sim 5\%$. The developed analytical theory can be used for the development and optimization of high-efficiency RF detectors and energy harvesters based on spintronic diodes.

With the advances of the Internet of Things and RFID technologies and wide application of micro- and nano-scale wireless devices that require independent power supplies, the problems of efficient RF signal detection and energy harvesting (EH) from ambient sources of radiation become critically important[1–5]. Both these problems can be solved with the help of spin-torque diodes (SDs) based on magnetic tunnel junctions (MTJs)[6–15]. In such a diode, input current $I(t) = I_{\rm RF}\cos(\omega t)$ subjected to an MTJ excites variations of the junction resistance $R(t)$ with angular frequency that is close to the current angular frequency $\omega = 2\pi f$. After the mixing of these resistance variations $R(t)$ with the input current $I(t)$ an output DC voltage $U_{\rm DC}$ across an MTJ is produced, $U_{\rm DC} = \langle I(t)R(t)\rangle$ (here we used ansatz $\langle x\rangle = T^{-1}\int_0^T x\,dt$, $T = 2\pi/\omega = 1/f$ is the period of the current oscillations)[6–8].

There are several possible regimes of operation of a SD[7,8]. Among them the most well known regime is the resonance regime, which is thoroughly studied in[6–12]. Another regime, the out-of-plane (OOP) regime (OOP-regime), where the SD works as a non-resonant threshold detector of low-frequency signals, is more suitable for broadband RF signal detection and EH[7,8,13–15]. In the OOP-regime, input RF current excites large-angle OOP magnetization precession in the free layer (FL) of an MTJ. In this case the diode's output DC voltage $U_{\rm DC}$ is negligibly small for input current magnitudes $I_{\rm RF}$ below some threshold $I_{\rm th}$. And the voltage $U_{\rm DC}$ is rather large and virtually does not depend on $I_{\rm RF}$, if $I_{\rm RF}$ exceeds the threshold $I_{\rm th}$. It was shown in[7,8,14] that the OOP-regime is observable at low signal frequencies f smaller than some threshold frequency $f_{\rm th}$.

In previous papers[7,8,14], the OOP-regime in a SD was studied, when a weak perpendicular bias DC magnetic field was applied to the diode having *isotropic* FL. In this article, however, we theoretically consider a more interesting type of a SD, where the FL has a *perpendicular magnetic anisotropy* (PMA) of the first and second order. It will be shown below that such a device can operate in the absence of bias DC magnetic field and provide rather large RF/DC power conversion efficiency in a wide frequency range.

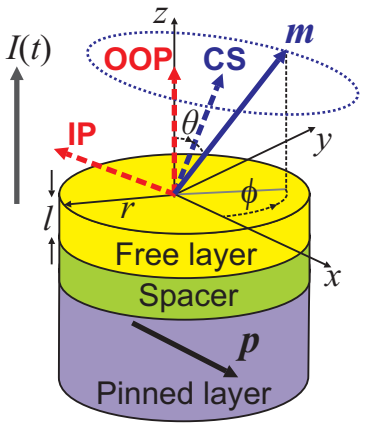

FIG. 1. (Color online) Model of the considered spin-torque diode (SD): circular nano-pillar of radius r consists of the free layer of thickness l, a spacer, and the pinned layer. Under the action of RF current $I(t)$ the unit magnetization vector $\boldsymbol{m}$ (solid blue arrow) is precessing along out-of-plane (OOP) trajectory (dashed blue curve) about the direction (dashed blue arrow) corresponded to the equilibrium cone state (CS) of the magnetization. The direction of magnetization for other two possible equilibrium states, the OOP and the in-plane (IP) states, are shown by red dashed arrows, respectively. $\boldsymbol{p} = \hat{\boldsymbol{x}}$ is the unit vector in the direction of the magnetization of the pinned layer, $\hat{\boldsymbol{x}}$ is the unit vector of x-axis.

We consider a SD formed by a circular MTJ nano-pillar (Fig. 1). We assume that the magnetization of the FL $\boldsymbol{M} = \boldsymbol{m}M_s$ is spatially uniform and depends on time t only (the macrospin approximation[16]), $\boldsymbol{m} \equiv \boldsymbol{m}(t)$ is the unit vector, and M_s is the saturation magnetization of the FL. The magnetization of the pinned layer is assumed to be completely fixed and its direction is defined by the unit vector $\boldsymbol{p} = \hat{\boldsymbol{x}}$, where $\hat{\boldsymbol{x}}$ is the unit vector of x-axis. The FL of an MTJ has a strong PMA of the first and second order[15], characterized by the anisotropy coefficients K_1 and K_2, respectively, and no in-plane

a)Electronic mail: Oleksandr.Prokopenko@gmail.com

anisotropy. There is no bias magnetic field applied to the structure, thus the effective magnetic field $\boldsymbol{B}_{\text{eff}}$ acting on the FL's magnetization $\boldsymbol{M}$ has contributions only from the demagnetization field[17] $-\hat{\boldsymbol{z}}\mu_0 M_s m_z$ and the PMA[15] $\hat{\boldsymbol{z}}\left[B_1 m_z + s_2 B_2 m_z\left(1-m_z^2\right)\right]$, where $\hat{\boldsymbol{z}}$ is the unit vector of z-axis, $m_z = \boldsymbol{m}\cdot\hat{\boldsymbol{z}}$, μ_0 is the vacuum permeability, $B_1 = 2K_1/M_s > 0$ and $B_2 = 4K_2/M_s > 0$ are the first- and second-order anisotropy fields, respectively, and $s_2 = \pm 1$ is the sign factor.

The magnetization dynamics in the FL is governed by the Landau-Lifshits-Gilbert-Slonczewski equation[7,8,18]:

$$\frac{d\boldsymbol{m}}{dt} = \gamma\left[\boldsymbol{B}_{\text{eff}}\times\boldsymbol{m}\right] + \alpha\left[\boldsymbol{m}\times\frac{d\boldsymbol{m}}{dt}\right] + \sigma I(t)\left[\boldsymbol{m}\times\left[\boldsymbol{m}\times\boldsymbol{p}\right]\right] , \quad (1)$$

where $\gamma \approx 2\pi\cdot 28$ GHz/T is the modulus of the gyromagnetic ratio, α is the Gilbert damping constant, $\sigma = \sigma_\perp/(1+\eta^2\cos\beta)$ is the current-torque proportionality coefficient, $\sigma_\perp = (\gamma\hbar/2e)\eta/(M_s V)$, $\hbar$ is the reduced Planck constant, e is the modulus of the electron charge, η is the spin-polarization of current, $V = \pi r^2 l$ is the volume of the FL (r is its radius and l is its thickness), and $\beta = \arccos(\boldsymbol{m}\cdot\boldsymbol{p})$ is the angle between the magnetizations of the free and pinned layers.

Using the expression $\boldsymbol{B}_{\text{eff}} = -(1/V)\partial E/\partial\boldsymbol{M}$ from Ref.[17], one can analyze the dependence of the magnetization energy E on m_z. It can be shown that there are three possible equilibrium magnetization states in the considered SD (see Fig. 1): the OOP state ($\boldsymbol{m} = \pm\hat{\boldsymbol{z}}$, $m_z = \pm 1$), the in-plane (IP) state ($\boldsymbol{m}$ lies in the x-y plane, $m_z = 0$), and the cone state (CS) that corresponds to the case $0 < |m_z| < 1$.

Among these three possible equilibrium magnetization states, the CS can be the most suitable state for broadband RF signal detection and EH due to the existence of optimal excitation conditions for the current-driven magnetization precession. This state can exist only when $B_1 < \mu_0 M_s$ and the sign factor $s_2 = +1$, thus, the effective magnetic field $\boldsymbol{B}_{\text{eff}}$ has its final form $\boldsymbol{B}_{\text{eff}} = \hat{\boldsymbol{z}}\left[-b_0 + B_2\left(1-m_z^2\right)\right]m_z$, where $b_0 = \mu_0 M_s - B_1 > 0$ is the "effective" first-order field that contributes from the first-order PMA field and the demagnetization field. A value of m_z that corresponds to the equilibrium CS of magnetization can be found as $m_{z,\text{CS}} = \pm\sqrt{1-\nu}$, where we introduced the field ratio $\nu = b_0/B_2$. Taking into account that m_z depends on the polar angle θ only ($m_z = \cos\theta$, see Fig. 1), one can estimate the equilibrium angle θ_{CS} that corresponds to the CS of magnetization: $\theta_{\text{CS}} = \arccos(\pm\sqrt{1-\nu})$. It can be seen that the equilibrium CS of magnetization is possible only when the second-order PMA field B_2 is stronger than the "effective" first-order field b_0. When $b_0 \to 0$ the CS transforms to the OOP state ($m_z \to \pm 1$), while at $b_0 \to B_2$ the CS turns into the IP state ($m_z \to 0$). Also it should be noted that due to the symmetry of the problem (states with $m_z > 0$ and $m_z < 0$ having the same absolute values of m_z are characterized by the same energy E), further we can consider only magnetization dynamics $\boldsymbol{m}(t)$ on the upper half of the unit sphere, hence, assuming $m_z > 0$.

We present the unit vector $\boldsymbol{m}$ in (1) in the form $\boldsymbol{m} = \hat{\boldsymbol{x}}\sin\theta\cos\phi + \hat{\boldsymbol{y}}\sin\theta\sin\phi + \hat{\boldsymbol{z}}\cos\theta$ ($\hat{\boldsymbol{y}}$ is the unit vector of y-axis) that allows one to write the equations for $d\theta/dt$ and $d\phi/dt$:

$$\frac{d\theta}{dt} = -\frac{\alpha\omega_p\sin\theta + \sigma I(t)\left(\alpha\sin\phi + \cos\theta\cos\phi\right)}{1+\alpha^2} , \quad (2a)$$

$$\frac{d\phi}{dt} = \frac{\omega_p - \sigma I(t)\left(\alpha\cot\theta\cos\phi - \csc\theta\sin\phi\right)}{1+\alpha^2} . \quad (2b)$$

Here $\theta \equiv \theta(t)$ and $\phi \equiv \phi(t)$ are the precession (polar) and azimuthal (in-plane) angles, respectively (see Fig. 1), $\omega_p \equiv \omega_p(\theta) = (\omega_2\sin^2\theta - \omega_0)\cos\theta$ is the frequency of the OOP precession, $\omega_0 = \gamma b_0$, $\omega_2 = \gamma B_2$, so $\nu = \omega_0/\omega_2$. Assuming that both the Gilbert damping constant α and input RF current magnitude I_{RF} are rather small, we can substantially simplify (2) by neglecting terms proportional to α^2 and αI_{RF}. However, this approach should not be used for the case of large-power input signals ($I_{\text{RF}} \gg I_{\text{th}}$)[19].

The next step in our analysis is to estimate the average influence of an input RF current on the magnetization dynamics. We assume that in the OOP-regime the magnetization precesses around some equilibrium inclined axis (corresponded to the equilibrium CS with the polar angle θ_{CS}) along approximately circular orbit (see Fig. 1). First, we let $\theta \approx$ const, $\phi \approx s\omega t + \psi$ in the CS, where ψ is the phase shift between the magnetization oscillations and the driving current, and the factor $s = \pm 1$ defines the direction of magnetization rotation. Second, we average the simplified equations for θ and ϕ over the period of oscillation $T = 2\pi/\omega$ of the driving current and obtain the following equations for the slow variables θ and ψ:

$$\left\langle\frac{d\theta}{dt}\right\rangle = -\alpha\omega_p\sin\theta - v\frac{\sigma_\perp I_{\text{RF}}}{2}\cos\theta\cos\psi , \quad (3a)$$

$$\left\langle\frac{d\psi}{dt}\right\rangle = \omega_p - s\omega + u\frac{\sigma_\perp I_{\text{RF}}}{2}\frac{1}{\sin\theta}\sin\psi . \quad (3b)$$

Here $u \equiv u(a_\eta) = (1-a_\eta^2)^{-1/2}\left[1 - (\sqrt{1-a_\eta^2}-1)^2/a_\eta^2\right]$ and $v \equiv v(a_\eta) = (1-a_\eta^2)^{-1/2}\left[1 + (\sqrt{1-a_\eta^2}-1)^2/a_\eta^2\right]$ are the dimensionless functions of parameter $a_\eta = \eta^2\sin\theta$. In typical experimental situation ($\eta \le 0.7$) the values of u and v are close to 1 for all angles θ.

The OOP-regime of magnetization precession corresponds to a stationary solution of (3): $\theta = \theta_s = $ const, $\psi = \psi_s = $ const. In this case one can find the stationary value of the phase shift ψ_s: $\sin\psi_s = (2/u)(s\omega - \omega_p)\sin\theta_s/\sigma_\perp I_{\text{RF}}$, $\cos\psi_s = (-2\alpha/v)\omega_p\tan\theta_s/\sigma_\perp I_{\text{RF}}$, and then obtain the characteristic equation for the stationary precession angle θ_s:

$$\left(\omega_p - s\omega\right)^2\sin^2\theta_s + \frac{u^2}{v^2}\alpha^2\omega_p^2\tan^2\theta_s = \frac{u^2}{2}\sigma_\perp^2\frac{P_{\text{RF}}}{R_0} . \quad (4)$$

Here $P_{\rm RF} = 0.5 I_{\rm RF}^2 R_0$ is the input RF power acting on the magnetization, and $R_0 = \langle R(t) \rangle$ is the equilibrium MTJ resistance.

Eq. (4) has solutions only for RF powers $P_{\rm RF}$ larger than a certain threshold power $P_{\rm th} = 0.5 I_{\rm th}^2 R_0$. Numerical analysis of (4) shows that the threshold power $P_{\rm th}$ mainly contributes from the second term in the left-hand side of the equation due to the quasi-resonant excitation of magnetization precession ($\omega_p \approx s\omega$). Taking this into account one can obtain an expression for the threshold power:

$$P_{\rm th} \approx 2 \left(\frac{\alpha}{v}\right)^2 \left(\frac{\omega}{\sigma_\perp}\right)^2 R_0 \tan^2 \theta_{\rm th} \ , \qquad (5a)$$

where the threshold angle $\theta_{\rm th}$ is a real-value solution of equation $\omega_p(\theta_{\rm th}) = s\omega$. Note, if one consider small oscillations of magnetization around its equilibrium state[20], one can obtain from (4) an analytical expression for $P_{\rm th}$:

$$P_{\rm th} \approx 2\alpha^2 \left(\frac{\omega}{\sigma_\perp}\right)^2 R_0 \frac{\nu}{v^2 (1-\nu) + \alpha^2 u^2} \ , \qquad (5b)$$

which is accurate at sufficiently low frequencies. Note that the threshold powers $P_{\rm th}$ defined from (5) do not depend on the direction of magnetization rotation (determined by the sign factor $s = \pm 1$) and vanish in the case $\omega \to 0$.

In order to analyze the stability of the magnetization precession in the OOP-regime around the CS of magnetization, we consider small deviations $\delta\theta$, $\delta\psi$ of variables θ, ψ near their stationary values θ_s and ψ_s, respectively. Using standard stability analysis technique for linearized equations with $\delta\theta$, $\delta\psi$, we found the two conditions of stability: (i) $d\theta/dI_{\rm RF} > 0$, and (ii) $6\sin^2\theta > 4 + \nu - \sqrt{4(2-\nu)^2 - 3\nu^2}$. The condition (i) determines the stable branch of solutions for θ, i.e. the branch for which the angle θ increases with current magnitude $I_{\rm RF}$. The condition (ii) is the condition on damping; it demonstrates that damping should increase with θ, so the precession orbit should remain stable, and hence, the OOP magnetization precession can be observable only for precession angles θ smaller than some critical angle defined by condition (ii).

Output DC voltage generated by a SD can be evaluated as $U_{\rm DC} = \langle I(t) R(t) \rangle = I_{\rm RF} R_\perp \langle \cos(\omega t)/[1 + \tau \cos\beta(t)] \rangle$, where $R(t) = R_\perp / [1 + \tau \cos\beta(t)]$ is the MTJ resistance[11,15], $R_\perp$ is the junction resistance for $\beta = \pi/2$, $\tau = {\rm TMR}/(2 + {\rm TMR})$, TMR is the tunneling magnetoresistance ratio of an MTJ, $\cos\beta(t) = \boldsymbol{m}(t) \cdot \boldsymbol{p} = \sin\theta_s \cos(s\omega t + \psi_s)$. Calculating analytically $\langle \cos(\omega t)/[1 + \tau \sin\theta_s \cos(s\omega t + \psi_s)] \rangle$ and using expression for $\cos\psi_s$, an output DC voltage can be written in a form

$$U_{\rm DC} = 2\alpha \frac{w}{v} R_\perp \frac{\omega_p}{\sigma_\perp} \tan\theta_s \approx w R_\perp \sqrt{\frac{2P_{\rm th}}{R_0}} \, . \qquad (6)$$

Here $R_0 = \langle R(t) \rangle = w_0 R_\perp$, $w \equiv w(a_\tau) = (1-a_\tau^2)^{-1/2}(1 - \sqrt{1-a_\tau^2})/a_\tau$ and $w_0 \equiv w_0(a_\tau) = (1-a_\tau^2)^{-1/2}$ are the dimensionless functions of parameter $a_\tau = \tau \sin\theta_s$. Also note that in the last expression for $U_{\rm DC}$ we used assumption $\omega_p \approx s\omega$.

As one can see, just above the threshold ($P_{\rm RF} \gtrsim P_{\rm th}$) output DC voltage $U_{\rm DC}$ of a SD virtually does not depend on the input RF power $P_{\rm RF}$ and linearly increases with the frequency ω (note that $\sqrt{P_{\rm th}} \sim \omega$). This regime of SD operation persists until $P_{\rm RF} > P_{\rm th}(\omega)$, i.e. while the signal frequency ω is smaller than some threshold frequency $\omega_{\rm th}$, which is defined from the equation $P_{\rm RF} = P_{\rm th}(\omega_{\rm th})$.

The EH efficiency ζ defined as a ratio between output DC power $P_{\rm DC} = U_{\rm DC}^2/R_0$ and input microwave power $P_{\rm RF} = 0.5 I_{\rm RF}^2 R_0$ can be written in a form

$$\zeta = \frac{P_{\rm DC}}{P_{\rm RF}} \approx 2 \left(\frac{P_{\rm th}}{P_{\rm RF}}\right) \left(\frac{w}{w_0}\right)^2 \, . \qquad (7)$$

For $P_{\rm RF} \geq P_{\rm th}$ the maximum value of ζ (achieved at the threshold) should be $\zeta_{\rm max} \approx 2(1 - \sqrt{1-a_\tau^2})^2/a_\tau^2$ that gives a maximum possible value of $\zeta_{\rm max} \approx 40\%$ calculated for the tunneling magnetoresistance ratio TMR of 600%[21]. But with a decrease of TMR the maximum value of EH efficiency $\zeta_{\rm max}$ substantially reduces, and, for instance, for TMR = 1 one can obtain only $\zeta_{\rm max} \approx 6\%$. In real experiments, however, measured values of ζ may be substantially smaller than the $\zeta_{\rm max}$ value due to the impedance mismatch[22] between an input transmission line with impedance $Z_{\rm TL}$ and a SD with impedance $Z_{\rm SD}$ connected to the line. To account this effect, one can use in (7) the effective input power delivered into the SD, $P_{\rm eff} = P_{\rm RF}(1 - |\Gamma|^2)$, instead of incident power $P_{\rm RF}$, where $\Gamma = (Z_{\rm SD} - Z_{\rm TL})/(Z_{\rm SD} + Z_{\rm TL})$ is the reflection coefficient[22].

For comparison of the developed theory with experimental data and results of numerical simulations we consider the case of the SD based on [PtMn(15)–$Co_{70}Fe_{30}$(2.3)–Ru(0.85)–$Co_{40}Fe_{40}B_{20}$(2.4)]/MgO(0.8)/ $Co_{20}Fe_{60}B_{20}$(1.65) MTJ (thicknesses in nm) with the following typical parameters (see[15] and supplementary to it): radius of the FL $r = 50$ nm, thickness of the FL $l = 1.65$ nm, normalized saturation magnetization of the FL $\mu_0 M_s = 1194$ mT, first order PMA field $B_1 = 1172$ mT, second order PMA field $B_2 = 64$ mT, Gilbert damping constant $\alpha = 0.02$, spin-polarization efficiency of current $\eta = 0.6$. From the values of B_1 and B_2, one can calculate the "effective" first-order field $b_0 = 22$ mT, the field or frequency ratio $\nu = b_0/B_2 = \omega_0/\omega_2 = 0.344$, z-component of the unit magnetization vector $\boldsymbol{m}$, $m_{z,\rm CS} = \sqrt{1-\nu} = 0.81$, and polar angle $\theta_{\rm CS} = \arccos m_{z,\rm CS} \approx 36°$ that correspond to the equilibrium CS of magnetization. Also using the values of MTJ resistance in parallel ($R_P = 640\ \Omega$) and antiparallel ($R_{AP} = 1236\ \Omega$) states and experimentally found tunneling magnetoresistance ratio TMR $= (R_{AP} - R_P)/R_P = 0.93$, one can calculate

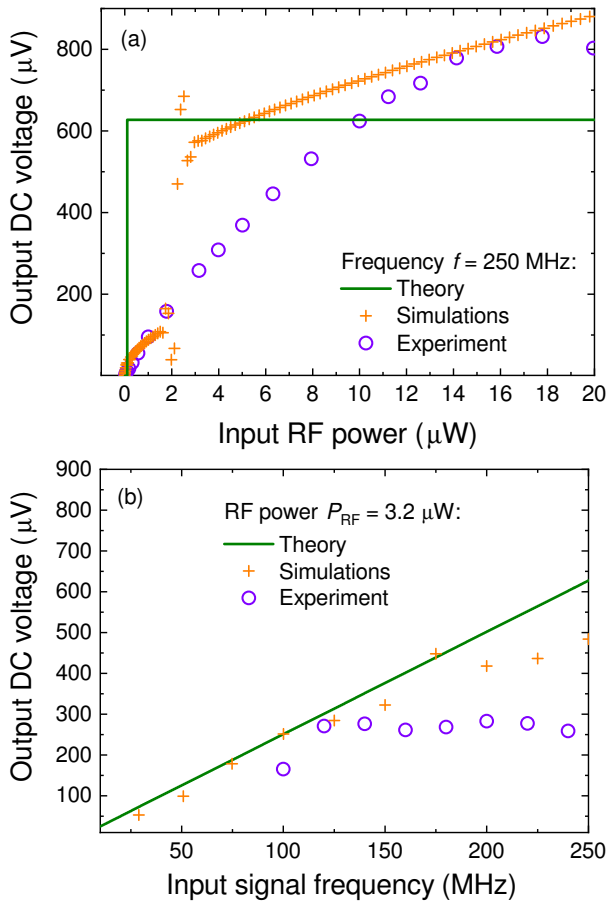

FIG. 2. (Color online) The dependence of the output DC voltage $U_{\rm DC}$ of a SD with chosen typical parameters on: (a) input signal power $P_{\rm RF}$ for the signal frequency of $f = 250$ MHz; (b) input signal frequency f with the power of $P_{\rm RF} = 3.2$ μW. Green solid lines are the analytical dependences given by Eq. (6). Cross points are the results of macrospin numerical simulations. Hollow violet circles corresponded to the experimental data from[15]. All other parameters are indicated in the text.

resistance of the SD in the perpendicular magnetic state ($\beta = \pi/2$) $R_\perp = 2R_{AP}R_P/(R_{AP} + R_P) = 843$ Ω.

To verify the theory we performed macrospin simulations[16] based on the numerical solution of (1) and then calculated the output DC voltage using a general expression $U_{\rm DC} = \langle I(t)R(t)\rangle$. The results obtained from the developed theory (green solid lines), from our simulations (cross points), and the experimental data (circle points) from paper[15] are shown in Fig. 2. As one can see, in the OOP-regime the SD works as a broadband non-resonant threshold RF detector. The response of the SD to an input RF power $P_{\rm RF}$ is non-zero and almost constant for RF powers $P_{\rm RF}$ that exceed frequency-dependent threshold power $P_{\rm th}$, thus, the power dependence of the output DC voltage $U_{\rm DC}$ has a step-like shape (green solid curve and cross points in Fig. 2(a)): $U_{\rm DC} \approx 0$ for $P_{\rm RF} < P_{\rm th}$ and $U_{\rm DC} \approx$ const for $P_{\rm RF} > P_{\rm th}$. The non-resonant response of the considered device to input RF signals with different signal frequencies f, demonstrated by the non-resonance dependence of $U_{\rm DC}(f)$ (Fig. 2(b)), can be observed only at low frequencies that are smaller than some threshold frequency $f_{\rm th}$: $U_{\rm DC}$ increases approximately linearly with the signal frequency f for $f < f_{\rm th}$ and $U_{\rm DC} \approx 0$ for $f > f_{\rm th}$. The existence of the threshold frequency $f_{\rm th}$ follows from Eq. (5) for the threshold power: with an increase of the signal frequency f, the threshold power $P_{\rm th}$ required for proper device operation also increases, and when this threshold power $P_{\rm th}$ reaches and then exceeds the input signal RF power $P_{\rm RF}$, magnetization oscillations in the device FL start to vanish.

The demonstrated behavior of a SD can be explained by a strong nonlinear frequency shift of the large-angle OOP magnetization precession[14,18,23]. During the change of power $P_{\rm RF}$ or frequency f of an input RF signal, the magnetization in the device FL "jumps" from one stable OOP-trajectory to another, but the precession frequency for these trajectories remains practically the same and is mainly determined by a large nonlinear frequency shift caused by the large precession amplitude[14,18].

It should be noted that although the theoretically and numerically calculated dependences of the output DC voltage $U_{\rm DC}$ on input signal power $P_{\rm RF}$ and signal frequency f, presented in Fig. 2, are in reasonable agreement, these dependences only satisfactory correspond to the experimental data from[15].First, in[15] almost linear dependence of $U_{\rm DC}$ on the signal frequency f is observed only at frequencies $\lesssim 100$ MHz that agrees with our theoretical and simulation results (see Fig. 2(b)). However, in the frequency range $f > 125$ MHz the experimentally measured DC voltage $U_{\rm DC}$ remains rather large and weakly depends on the frequency f in contrast to the developed theory that predicts $U_{\rm DC} \sim f$ for $f < f_{\rm th}$. Second, the power dependence of the output DC voltage $U_{\rm DC}(P_{\rm RF})$ measured in the experiment[15] at the signal frequency of 250 MHz has a similar, but blurred a step-like shape as predicted by the theory (see Fig. 2(a)). Thus, the developed theory is able to qualitatively explain the experimental results[15] only in the range of sufficiently low frequencies. We believe that some discrepancy between the experiment[15] and the theory, could be explained by an influence of in-plane anisotropy in the experiment and by the transition of the OOP magnetization precession around the equilibrium CS of magnetization in the diode's FL to a different magnetization precession regime, which requires an additional study.

Also it is important to note, that the efficiency ζ of RF/DC energy conversion for the SD with chosen typical parameters, calculated from the data of our numerical simulations, reaches 5.7% at the threshold that well agrees with the theoretical dependence (7). If we take into account the impedance mismatch effect discussed above, ζ reduces down to 1.5%, but still remains rather large for some practical applications.

In conclusion, we have shown theoretically that a spin-torque diode (SD) having a first and second order perpen-

dicular magnetic anisotropy of the free layer can be used as an efficient RF signal detector and energy harvester operating in the absence of a bias DC magnetic field. The device generates a non-zero output DC voltage, when the input RF power $P_{\rm RF}$ subjected to the SD exceeds a frequency-dependent power threshold $P_{\rm th}$, and the voltage weakly depends on power for powers $P_{\rm RF} > P_{\rm th}$. Such a regime of diode operation is possible at low frequencies below the threshold frequency dependent of RF signal power and/or device geometry. Finally, it was demonstrated that the energy harvesting efficiency for such a harvester could exceed 5% (1.5% with an account of the impedance mismatch effect) that is sufficient for some practical applications.

This work was supported in part by the grants Nos. 18BF052–01M and 19BF052–01 from the Ministry of Education and Science of Ukraine and grant No. 1F from the National Academy of Sciences of Ukraine.

[1] A. Harb, Renew. Energy **36**, 2641 (2011).
[2] Y. Duroc, G. Andia Vera, Towards Autonomous Wireless Sensors: RFID and Energy Harvesting Solutions, in: S.C. Mukhopadhyay (Ed.), *Internet of Things: Challenges and Opportunities* (Smart Sensors, Measurement and Instrumentation, Vol. 9) (Springer, Berlin, 2014).
[3] C.R. Valenta and G.D. Durgin, IEEE Microw. Mag. **15**, 108 (2014).
[4] S.K. Divakaran, D.D. Krishna, Nasimuddin, Int. J. RF Microw. Comput. Aided Eng. **29**, e21633 (2019).
[5] B. Pozo, J.I. Garate, J.Á. Araujo and S. Ferreiro, Electronics **8**, 486 (2019).
[6] A.A. Tulapurkar, Y. Suzuki, A. Fukushima *et al.*, Nature **438**, 339 (2005).
[7] O.V. Prokopenko, I.N. Krivorotov, T.J. Meitzler *et al.*, Spin-Torque Microwave Detectors, in: S.O. Demokritov and A.N. Slavin (Eds.), *Magnonics: From Fundamentals to Applications* (Topics in Applied Physics, Vol. 125) (Springer, Berlin, 2013).
[8] O.V. Prokopenko and A.N. Slavin, Low Temp. Phys. **41**, 353 (2015).
[9] S. Ishibashi, T. Seki, T. Nozaki *et al.*, Appl. Phys. Express **3**, 073001 (2010).
[10] O. Prokopenko, G. Melkov, E. Bankowski *et al.*, Appl. Phys. Lett. **99**, 032507 (2011).
[11] S. Miwa, S. Ishibashi, H. Tomita *et al.*, Nature Mater. **13**, 50 (2014).
[12] B. Fang, M. Carpentieri, X. Hao *et al.*, Nature Commun. **7**, 11259 (2016).
[13] X. Cheng, C.T. Boone, J. Zhu, and I.N. Krivorotov, Phys. Rev. Lett. **105**, 047202 (2010).
[14] O.V. Prokopenko, I.N. Krivorotov, E. Bankowski *et al.*, J. Appl. Phys. **111**, 123904 (2012).
[15] B. Fang, M. Carpentieri, S. Louis *et al.*, Phys. Rev. Applied **11**, 014022 (2019).
[16] In[15] it was shown that the SD's FL has a single domain magnetic state, so the use of macrospin approximation is acceptable.
[17] A.G. Gurevich and G.A. Melkov, *Magnetization Oscillations and Waves* (CRC Press, New York, 1996).
[18] A. Slavin and V. Tiberkevich, IEEE Trans. Magn. **45**, 1875 (2009).
[19] R. Tomasello, B. Fang, P. Artemchuk *et al.*, Low frequency non-resonant rectification in spin-diodes, submitted to Phys. Rev. Appl. (2020).
[20] We consider small oscillations of magnetization around its equilibrium state assuming that $\theta_s = \theta_{\rm CS} + \Delta\theta$, where $\theta_{\rm CS}$ is the equilibrium angle, and $\Delta\theta$ is a small angle deviation, which can be positive or negative. We express $\omega_p(\theta_s)$ as $\omega_p(\theta_s) \approx [\partial\omega_p(\theta_{\rm CS})/\partial\theta]\Delta\theta = 2\omega_2(1-\nu)\sqrt{\nu}\Delta\theta$ and use approximations $\sin\theta_s \approx \sin\theta_{\rm CS}$, $\tan\theta_s \approx \tan\theta_{\rm CS} + \Delta\theta/\cos^2\theta_{\rm CS}$. Then after retaining in the equation for $\Delta\theta$ obtained from (4) only terms that are independent of $\Delta\theta$ and terms proportional to $\Delta\theta$ or $\Delta\theta^2$, one can solve it and find an approximate expression (5b) for the threshold power $P_{\rm th}$.
[21] S. Ikeda, J. Hayakawa, Y. Ashizawa *et al.*, Appl. Phys. Lett. **93**, 082508 (2008).
[22] D.M. Pozar, *Microwave Engineering*, fourth ed. (John Wiley & Sons, New York, 2012).
[23] K. Kudo, T. Nagasawa, R. Sato, and K. Mizushima, Appl. Phys. Lett. **95**, 022507 (2009).